

Article

Numerical Simulation of Hydraulic Fracture Propagation Guided by Single Radial Boreholes

Tiankui Guo *, Zhanqing Qu, Facheng Gong and Xiaozhi Wang

College of Petroleum Engineering, China University of Petroleum, Huadong, Qingdao 266580, China; quzhq@upc.edu.cn (Z.Q.); 18754257325@163.com (F.G.); wxz666168@163.com (X.W.)

* Correspondence: guotiankui@126.com; Tel.: +86-183-6629-2020

Received: 11 September 2017; Accepted: 20 October 2017; Published: 23 October 2017

Abstract: Conventional hydraulic fracturing is not effective in target oil development zones with available wellbores located in the azimuth of the non-maximum horizontal in-situ stress. To some extent, we think that the radial hydraulic jet drilling has the function of guiding hydraulic fracture propagation direction and promoting deep penetration, but this notion currently lacks an effective theoretical support for fracture propagation. In order to verify the technology, a 3D extended finite element numerical model of hydraulic fracturing promoted by the single radial borehole was established, and the influences of nine factors on propagation of hydraulic fracture guided by the single radial borehole were comprehensively analyzed. Moreover, the term ‘Guidance factor (G_i)’ was introduced for the first time to effectively quantify the radial borehole guidance. The guidance of nine factors was evaluated through gray correlation analysis. The experimental results were consistent with the numerical simulation results to a certain extent. The study provides theoretical evidence for the artificial control technology of directional propagation of hydraulic fracture promoted by the single radial borehole, and it predicts the guidance effect of a single radial borehole on hydraulic fracture to a certain extent, which is helpful for planning well-completion and fracturing operation parameters in radial borehole-promoted hydraulic fracturing technology.

Keywords: radial borehole; hydraulic fracturing; fracture propagation; Abaqus; numerical simulation

1. Introduction

The term radial borehole (also known as radial well) refers to a horizontal borehole with a radius far smaller than that of conventional drilling holes, and its borehole is formed mostly by a hydraulic jet, with a length between 10 m and 100 m and a borehole diameter between 25 mm and 50 mm [1–4]. The reservoir simulation technology of radial boreholes combined with hydraulic fracturing is an innovative technology to effectively develop low-permeability, thin-layer, fractured reservoirs, water-flooded ‘dead oil areas’ and lithologic trap reservoirs [5,6].

By means of radial boreholes, we can make hydraulic fractures overcome the control of the original in-situ stress to some extent, and realize the artificial control of directional propagation toward the target zone (shown in Figure 1), but because the guiding strength of a single radial drilling is limited, it is possible that the hydraulic fracture does not propagate along the orientation of the radial borehole, and instead, a deflection occurs midway, which results in an unsatisfactory stimulation effect. At present, due to the lack of any relevant theory, the technological parameters of hydraulic fracturing guided by the single radial well are usually difficult to design scientifically, so the success rate is low and the application of this technology is greatly limited.

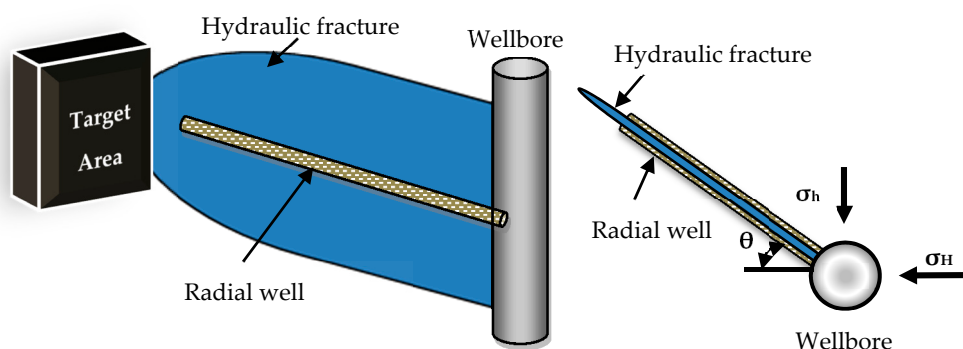


Figure 1. Schematic diagram of hydraulic fracture-directed propagation guided by a single radial well.

Currently, fracture propagation mechanism research on hydraulic fracturing guided by a single radial borehole has not been reported, but there are relatively more studies on the initiation position and pressure of perforated wellbores [7] and fracture propagation guided by directional perforation. However, the differences in length, diameter and density lead to a significant difference in the guidance effect on hydraulic fractures between radial boreholes and perforations.

For perforation, Cherny et al. [8] thought that 2D and pseudo-3D approaches for fracture initiation modeling were insufficient for the description of the near wellbore effects. The complicated geometrical configuration of perforated wellbores required the consideration of the fracture initiation process in a 3D model. The initiation pressure, location and direction of the fracture were fully determined by the stress state in the vicinity of the wellbore and the perforation. Yuan et al. [9] used the 3D finite element method (FEM) to establish a model of a wellbore with two identical perforations, and the stress analysis was performed for different wellbore azimuth conditions. The research showed that the area of influence of the perforations was limited to a distance of 6–8 times the perforation diameter. Alekseenko et al. [10] used the 3D BEM to establish a fracture initiation model for perforated non-cemented wellbores. The analysis of fracture initiation location and pressure was performed for different perforating parameters for vertical and horizontal wells, but the subsequent fracture propagation was not studied. Zhu et al. [11] established a prediction model of hydraulic fracture initiation guided by directional perforation, and analyzed the influence of directional perforation on initiation pressure and fracture form. A true triaxial hydraulic fracturing experiment was conducted by Lei et al. [12] who studied the influence of perforation spacing and horizontal in-situ stress differences on hydraulic fracture propagation, and thought that more perforation holes and smaller in-situ stress difference benefited propagation of fracture along the perforation direction. A hydraulic fracturing experiment for tight sandstone was conducted by Fallahzadeh et al. [13] who found that both boreholes and perforations affect the initiation mechanism of tight reservoirs, and perforations affect the geometrical morphology of hydraulic fractures in the immediate vicinity of the wellbore. Through massive fracturing experiments, Chen et al. [14] thought that the change of directional perforation angle and horizontal in-situ stress differences influenced the propagation of hydraulic fractures. Based on the hydraulic fracturing experiments guided by directional perforations, Hong et al. [15] studied the guidance effect of perforation number on hydraulic fractures, and thought that a sufficient number of guideholes created an effective crack, which promoted the initiation and propagation of hydraulic fracture.

Based on extended finite element theory, a 3D numerical model of hydraulic fracturing guided by a single radial borehole was established [16–23] by Abaqus Software. It revealed the effects of horizontal in-situ stress differences, azimuths, diameters and lengths of radial borehole, injection rate and viscosity of the fracturing fluid, Young modulus and Poisson's ratio of rock, and reservoir permeability on the guidance strength of the single radial borehole to hydraulic fracture propagation, and provided a scientific basis for effective operation of hydraulic fracturing guided by a single radial borehole. Thus, the problems that the hydraulic fracture only extends along the direction parallel to

horizontal maximum in-situ stress, which causes available wellbores to fail to develop the remaining oil and trap reservoir, and complex multi-fractures tend to generate in the immediate vicinity of wellbores, which makes it hard to realize deep fracture penetration, were solved. This may improve the effect of fracturing operation and recovery efficiency. Furthermore, the study has also important reference value for increasing the stimulated volume of unconventional reservoirs by using the guidance of multi-radial boreholes or enhancing the control of fracture shape in geothermal systems [24,25].

2. Establishment of a Fluid-Solid Coupling Mathematical Model and Its Finite Element Discretization

2.1. Stress Balance Equation

The stress balance equation of rock porous media can be obtained by the virtual work principle. At some point, the rock's virtual work is equal to the virtual work generated by the physical and facial forces acting on the rock. Without considering the fluid viscosity in the rock, the final formula can be obtained [26,27]:

$$\int_V \delta \boldsymbol{\varepsilon}^T \mathbf{D}_{ep} \frac{d\boldsymbol{\varepsilon}}{dt} dV + \int_V \delta \boldsymbol{\varepsilon}^T \mathbf{D}_{ep} \left[\mathbf{m} \frac{(s_o + p_o \boldsymbol{\varepsilon}) dp_o}{3K_s dt} \right] dV - \int_V \delta \boldsymbol{\varepsilon}^T \mathbf{m} (s_o + p_o \boldsymbol{\xi}) \frac{dp_o}{dt} dV = \int_V \delta \mathbf{u}^T \frac{d\mathbf{f}}{dt} dV + \int_S \delta \mathbf{u}^T \frac{d\boldsymbol{\tau}}{dt} dS \quad (1)$$

where \mathbf{D}_{ep} is the elastic-plastic matrix, t is the time, $\mathbf{m} = [1, 1, 1, 0, 0, 0]^T$, K_s is the compressive modulus of solid particles, s_o is the liquid saturation of the rock, $\boldsymbol{\xi} = ds_o/dp_o$ is the parameter characterizing the relationship between capillary pressure and saturation, p_o is the pore liquid pressure, $\boldsymbol{\tau}$ is the rock facial force, \mathbf{f} is the rock physical force, $\delta \boldsymbol{\varepsilon}$ the virtual displacement, $\delta \mathbf{u}$ is the virtual strain, dV is the volume micro-element, dS is the area micro-element.

2.2. Continuity Equation

For a certain volume of rock, from the mass conservation theorem, it is known that the mass of fluid flowing into the rock is equal to the sum of the internal fluid increase and the fluid outflow during a certain period of time. Assuming that the seepage law in the rock is Darcy percolation, the law of Darcy percolation could be used to express this process, and the continuity equation of fluid seepage can be obtained by deduction [26,27]:

$$s_o \left(\mathbf{m}^T - \frac{\mathbf{m}^T \mathbf{D}_{ep}}{3K_s} \right) \frac{d\boldsymbol{\varepsilon}}{dt} - \nabla^T \left[\mathbf{k}_0 \mathbf{k}_r \left(\frac{\nabla p_o}{\rho_o} - \mathbf{g} \right) \right] + \left\{ \boldsymbol{\xi} n + n \frac{s_o}{K_o} + s_o \left[\frac{1-n}{3K_s} - \frac{\mathbf{m}^T \mathbf{D}_{ep} \mathbf{m}}{(3K_s)^2} \right] (s_o + p_o \boldsymbol{\xi}) \right\} \frac{dp_o}{dt} = 0 \quad (2)$$

where \mathbf{k}_0 is the product of the initial permeability coefficient tensor and the fluid density, ρ_o is the liquid density, \mathbf{k}_r is the specific permeability coefficient, \mathbf{g} is the vector form of gravity acceleration, n is the porosity of the rock, K_o is the volume modulus of the liquid in the rock.

2.3. Boundary Conditions

(1) Traffic boundary conditions [27]

$$-\mathbf{n}^T \mathbf{k} \mathbf{k}_r \left(\frac{\nabla p_o}{\rho_o} - \mathbf{g} \right) = q_o \quad (3)$$

where \mathbf{n} is the unit normal direction of the flow boundary, \mathbf{k} is the permeability coefficient tensor, q_o is the total liquid volume flowing through the boundary per unit time.

(2) Pore pressure boundary conditions

Pore pressure boundary conditions can be expressed by $p_o = p_{ob}$, that is, the boundary pressure is a certain value p_{ob} .

(3) Position boundary conditions

Constrain the displacement of the boundary nodes in the X and Y direction, $U_x = 0, U_y = 0$.

2.4. Finite Element Discretization Method and Stress-Seepage Coupling Equation

Define the shape function for [27]:

$$\left. \begin{aligned} \mathbf{u} &= \mathbf{N}_u \bar{\mathbf{u}} \\ \boldsymbol{\varepsilon} &= \mathbf{B} \bar{\mathbf{u}} \\ p_o &= \mathbf{N}_p \bar{p}_o \end{aligned} \right\} \quad (4)$$

where \mathbf{N}_u and \mathbf{B} is the vector matrix of the shape function, $\bar{\mathbf{u}}$ is the unit node displacement, \bar{p}_o is the unit node pore pressure, \mathbf{N}_p is the shape function:

$$\int_V \mathbf{a}^T \bar{A} dV + \int_S \mathbf{b}^T \bar{B} dS = 0 \quad (5)$$

where \bar{A} is the control equation, \bar{B} is the continuous boundary equation.

Substituting Equation (4) into Equation (1), the solid-state finite element formula is obtained by simplification:

$$\mathbf{K} \frac{d\bar{\mathbf{u}}}{dt} + \mathbf{C} \frac{d\bar{p}_o}{dt} = \frac{d\mathbf{f}}{dt} \quad (6)$$

By moving the Equations (2) and (3), let the right side of the equation be 0. Then the Galerkin method is used to make the left polynomials of the Formulas (2) and (3) respectively to substitute \bar{A} and \bar{B} of Equation (5), and substitute the shape function constructed by $\boldsymbol{\varepsilon}$ and p_o in Equation (4) into Equation (5). Making $\mathbf{a} = -\mathbf{b}$, the deformation formula is simplified as follows:

$$\mathbf{E} \frac{d\bar{\mathbf{u}}}{dt} + \mathbf{F} \bar{p}_o + \mathbf{G} \frac{d\bar{p}_o}{dt} = \hat{\mathbf{f}} \quad (7)$$

The stress-seepage coupling Equation (8) can be obtained by the simultaneous the Formulas (6) and (7), this equation can be solved through the ABAQUS finite element solver. The distribution law of the related parameters, such as stress, strain, displacement, porosity, permeability and saturation, etc., in the concern area can be obtained:

$$\begin{bmatrix} \mathbf{K} & \mathbf{C} \\ \mathbf{E} & \mathbf{G} \end{bmatrix} \frac{d}{dt} \begin{Bmatrix} \bar{\mathbf{u}} \\ \bar{p}_o \end{Bmatrix} + \begin{bmatrix} 0 & 0 \\ 0 & \mathbf{F} \end{bmatrix} \begin{Bmatrix} \bar{\mathbf{u}} \\ \bar{p}_o \end{Bmatrix} = \begin{Bmatrix} \frac{d\mathbf{f}}{dt} \\ \hat{\mathbf{f}} \end{Bmatrix} \quad (8)$$

Of which:

$$\begin{aligned}
 \mathbf{K} &= \int_V \mathbf{B}^T \mathbf{D}_{ep} \mathbf{B} dV \\
 \mathbf{C} &= \int_V \mathbf{B}^T \mathbf{D}_{ep} \mathbf{m} \frac{(s_o + \xi p_o)}{3K_s} N_p dV - \int_V \mathbf{B}^T (s_o + \xi p_o) \mathbf{m} N_p dV \\
 \mathbf{E} &= \int_V N_p^T \left[s_o \left(\mathbf{m}^T - \frac{\mathbf{m}^T \mathbf{D}_{ep}}{3K_s} \right) \mathbf{B} \right] dV \\
 \mathbf{F} &= \int_V (\nabla N_p)^T \mathbf{k} \mathbf{k}_t \nabla N_p dV \\
 \mathbf{G} &= \int_V N_p^T \left\{ s_o \left[\left(\frac{1-n}{K_s} - \frac{\mathbf{m}^T \mathbf{D}_{ep} \mathbf{m}}{(3K_s)^2} \right) \cdot (s_o + p_o \xi) + \xi n + n \frac{s_o}{K_o} \right] \right\} N_p dV \\
 \mathbf{d}\mathbf{f} &= \int_V N_u^T \mathbf{d}\mathbf{f} dV + \int_S N_u^T \mathbf{d}\tau dS \\
 \tilde{\mathbf{f}} &= \int_S N_p^T q_{ob} dS - \int_V (\nabla N_p)^T \mathbf{k} \mathbf{k}_t \mathbf{g} dV
 \end{aligned} \tag{9}$$

where q_{ob} is the fluid flow on the boundary.

3. Numerical Simulation of Propagation of Hydraulic Fracture

3.1. Introduction to the Model

3.1.1. Simulation of Initial Fracture

The enrichment functions are introduced to finite element approximation to simulate initial fracture, and the fracture discontinuity is described by the enrichment functions related with the additional degree of freedom. The displacement vector function \mathbf{u} characterizing entire division is written as [28]:

$$\mathbf{u} = \sum_{I=1}^N N_I(\mathbf{x}) [\mathbf{u}_I + H(\mathbf{x}) \mathbf{a}_I + \sum_{\alpha=1}^4 F_{\alpha}(\mathbf{x}) \mathbf{b}_I^{\alpha}] \tag{10}$$

where $N_I(\mathbf{x})$ is the shape-function of general nodal displacement, \mathbf{u}_I is the continuous part of the solution to displacement, both \mathbf{a}_I and \mathbf{b}_I^{α} are nodal extended freedom degree vectors, $H(\mathbf{x})$ is the discontinuity jump function, $F_{\alpha}(\mathbf{x})$ represents the stress asymptotic function in the tip of a crack.

3.1.2. Level-Set Simulation of Fracture Propagation

The level-set method, a powerful numerical analysis technique, could simulate and calculate the movement of a fracture interface, without regeneration of gridding. The ϕ function is renewed by computing zero level set of Ψ and ϕ_i (crack terminal point function) to simulate fracture propagation. Renewal and evolution of ϕ is actually a progress of simulating the fracture propagation [29]. The nodal value of enrichment function is determined by two level-set functions, as shown in Figure 2.

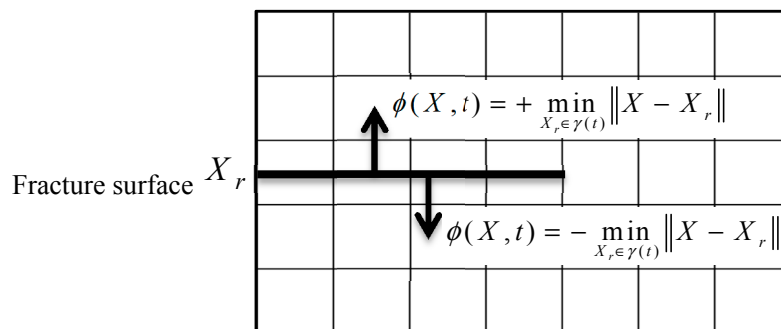


Figure 2. Schematic diagram of fracture surface simulation and level set function on the calculation point.

Generally, the symbol distance function in level-set method is written as:

$$\phi(X, t) = \pm \min_{X_r \in \gamma(t)} \|X - X_r\| \quad (11)$$

where $\phi(X, t)$ is to describe the fracture interface. When point X is located above the fracture defined by $\gamma(t)$, the value of the equation is positive, and vice versa.

3.1.3. Criteria for Initiation of Fracture

At present, the common criteria in the finite-element analytic method for judging initiation of fractures include the maximum principal stress, maximum principal strain, maximum normal stress, maximum principal strain, double-step traction influence, etc. [27,30]. It is thought after a large amount of working and simulation, that the maximum principal stress provides a higher stability, better convergence during computation and stronger compatibility for judging initiation of fracture.

The maximum principal stress criterion is written as:

$$f = \left\{ \frac{\langle \sigma_{\max} \rangle}{\sigma_{\max}^a} \right\} \quad (12)$$

where σ_{\max}^a is critical maximum principal stress, $\langle \rangle$ indicates that Macaulay thought that there is no initial loss for model when affected by compression stress. When the maximum stress ratio reaches a certain critical value, damage to the model occurs.

3.1.4. Damage Evolution Law

Damage theory was first proposed by Kachanov [31] for the study of metal creep. The damage references the progressive weakening of internal material cohesion, which leads to the destruction of the unit volume. It presents a gradual degradation of the carrier material results from emergence and development of the micro-defects (microcracks and microvoids). Damage is generally used as a "deterioration factor" to incorporate into the elastic, plastic and viscoplastic media. Due to irreversible changes in the damage development and material structure, scholars have used different definitions of damage [26]. The average damage of fracture units is defined as "D" in this paper. A scalar damage variable, D , represents the averaged overall damage at the intersection between the crack surfaces and the edges of cracked elements. It initially has a value of 0. If damage evolution is modeled, D monotonically evolves from 0 to 1 upon further loading after the initiation of damage. If $D = 1$, it shows that the material unit is completely broken. The influence of damage on normal and shear stress components is expressed as:

$$t_n = \begin{cases} (1-D)T_n, T_n \geq 0 \\ T_n, T_n < 0 \end{cases} \quad (13)$$

$$t_s = (1-D)T_s \quad (14)$$

$$t_t = (1-D)T_t \quad (15)$$

where T_n , T_s and T_t are the normal and shear stress components predicted by the elastic traction-separation behavior for the current separations without damage. t_n , t_s and t_t are the actual withstand stresses in the three corresponding directions.

3.1.5. Energy Release Rate Criterion

Introducing the energy release rate 'G', the damage evolution of fracture is determined based on the Benzeggagh-Kenane (B-K) criteria [32] and expressed as:

$$G_n^C + (G_s^C - G_n^C) \left\{ \frac{G_s}{G_T} \right\}^\eta = G^C \quad (16)$$

where G_n^C and G_s^C are the normal and tangential fracture critical energy release rate, respectively, G_s and G_T are the two tangential fracture energy release rates. The two tangential energy release rates are considered to be equal in the B-K criterion. η is a constant related to the material properties. G^C is the fracture critical energy release rate of composite crack. When the energy release rate calculated at the crack tip node is greater than the B-K critical energy release rate, the current crack tip node of the cohesive unit will unlock the binding section, and the crack extends forward.

3.1.6. Solution

Modeling and mesh generation are operated in the Abaqus software, and fluid-solid coupling during hydraulic fracturing is simulated by its inherent Module Soil. Fracture propagation is simulated by the XFEM-based Cohesive Zone Model (CZM) in Abaqus [33]. CZM is applicable in XFEM to quantify the magnitude of the discontinuity, the displacement jump across the fracture faces, and to establish fracture initiation and propagation criteria using mixed-mode formulae such as BK law. Moreover, formula integration is reduced using bilinear displacement of quadrangle plain stress, and an hour glass is introduced to control convergence of computation and operate multi-threading computation.

3.2. Assumptions

- (1) Only a strip of hydraulic fracture is generated during fracturing, which is initiated along the azimuth of the radial borehole [34].
- (2) The formation rock is isotropic.

3.3. Fundamental Parameters of Model

Taking Well x in the Shengli Oilfield (shown in Table 1) for example, a 3D cylindrical numerical model of the oil reservoir with a radius of 20 m and thickness of 1.5 m is established to simulate fracture propagation under the conditions of different rock physical and mechanical properties and operation parameters.

Table 1. Basic parameters of the X Well in the Shengli Oilfield.

Parameters	Value	Parameters	Value
Reservoir saturation	1	Poisson ratio of rock	0.25
Initial pore pressure	20 MPa	Young's modulus of rock	12.9 GPa
Initial porosity	0.16	Reservoir permeability	$60 \times 10^{-3} \mu\text{m}^2$
Horizontal maximum principal stress (σ_H)	41 MPa	Filtration coefficient	$10^{-10} \text{ m s}^{-1}$
Horizontal minimal principal stress (σ_h)	36 MPa	Injection rate of fracturing fluid	$3.2 \text{ m}^3 \text{ min}^{-1}$
Overburden stress	45 MPa	Fracturing fluid viscosity	50 mPa·s
Tensile strength of rock	3.0 MPa	Fracturing fluid density	9525 kg/m ³
Casing diameter	139.7 mm	Reservoir model size (diameter)	40 m

4. Analysis of Simulation Results

4.1. Azimuth of Radial Borehole

Two numerical models (Figure 3) with same parameters are established based on the parameters in Table 1. The radial borehole is not established in Model A, and the single radial borehole with hole diameter of 0.05 m, and well length of 20 m is established in Model B. The azimuth of a radial borehole is the angle between the orientation of the radial borehole and horizontal maximum principal stress. In Model A, the hydraulic fracture without the guidance of radial borehole propagates along maximum principal stress (X direction), which is shown in Figure 4. In Model B, affected by stress interference, the propagation trajectory of the hydraulic fracture guided by a radial borehole has

changed, which is shown in Figure 5. The concept of “guidance factor (G_f)” is introduced to characterize the guidance of the radial borehole on a hydraulic fracture. The guidance factor “ G_f ” is defined as the ratio of the area surrounding a hydraulic fracture and radial borehole and its round boundary to the whole flat area in a 2D plane in bird’s-eye view, namely $G_f = S_p/S$ in Figure 6.

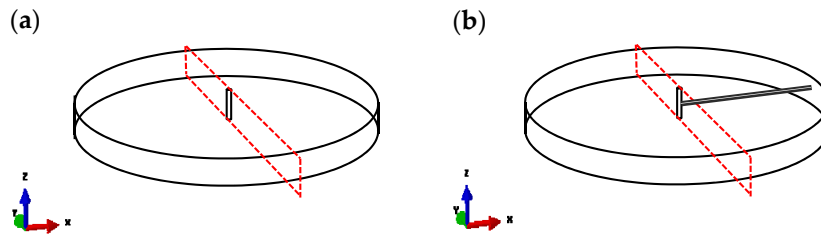


Figure 3. Wireframe view: (a) A model without radial well and (b) B model with the single radial well.

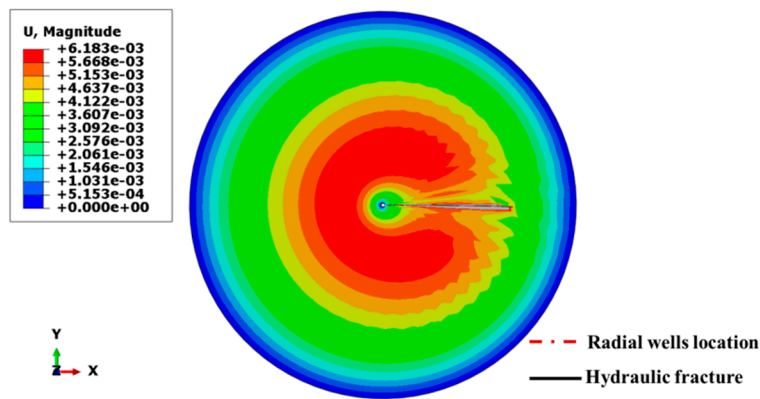


Figure 4. Simulation result of hydraulic fracture propagation without the guidance of radial well.

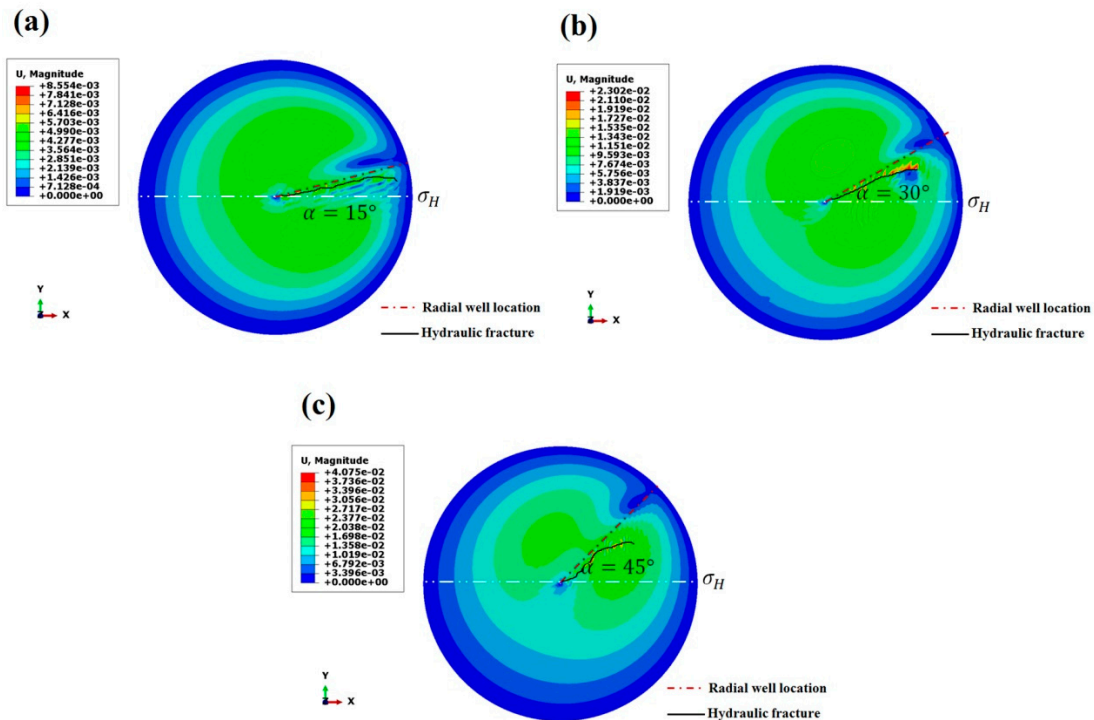


Figure 5. Simulation results of hydraulic fracture propagation guided by the single radial well in different azimuths: (a) 15°; (b) 30°; and (c) 45°.

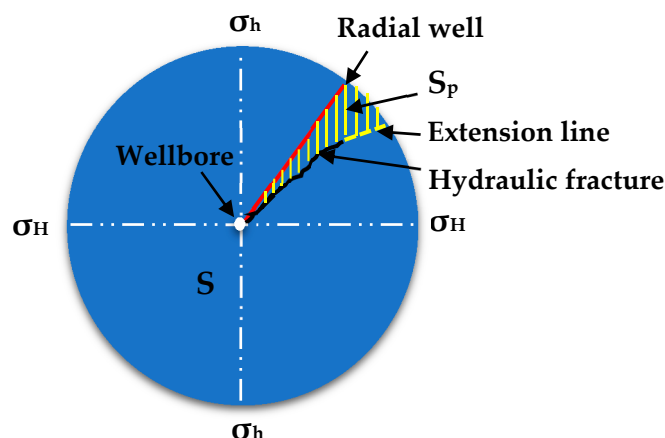


Figure 6. Schematic diagram of the guiding factor “ G_f ”.

S_p is the area surrounding the hydraulic fracture and radial borehole and its round boundary, and S is total area of 2D plane of reservoir model. During numerical simulation, the circular boundary restrains the displacement in three directions. A hydraulic fracture will stop propagating when it extends to the boundary, but there may be some distance between the front end of the hydraulic fracture and the model boundary. Only through establishment of a hydraulic fracture extension line based on the late propagation trend, the area (S_p) surrounded by hydraulic fracture (and extension line), radial borehole and the round boundary can be calculated. Using the lasso tool of “Adobe Photoshop” software, you can select the area with any shape (S_p) that needs to be calculated, and then get the pixels of the selected area, the pixels ratio of two areas “ S_p ” and “ S ” is G_f . The use of the pixel calculation method is very accurate and convenient. G_f is between 0 and 0.25, and a lower value indicates a stronger guidance of the radial borehole on the hydraulic fracture.

In the hydraulic fracturing process, the radial borehole filled with fracturing fluid will produce stress interference at a certain range of formation around the borehole, which is also the reason for fracture propagation along the radial borehole direction. Based on this study model, a large number of numerical simulation results show that this radius of stress interference is about 2 m. Therefore, by calculating the vertical distance between the hydraulic fracture and the radial borehole, it is considered that the hydraulic fracture significantly deflected from the radial borehole when this vertical distance exceeds 2 m. At this time, we can also observe the occurrence of a relatively significant deviation from the picture. The distance from the origin to the position where the deflection occurs is the so-called extending distance along the radial borehole orientation. We intend to use the “the extending distance along orientation of radial borehole” as another quantitative evaluation parameter.

When a hydraulic fracture propagates along the direction of a radial borehole, G_f is 0, which has the best guidance. When the angle between the hydraulic fracture and radial borehole is 90° , G_f is 0.25, which means no guidance. A large amount of numerical simulation shows that it is valid to use the guidance factor G_f to determine the guidance strength of a radial borehole on a hydraulic fracture. In Model B, the guidance factors corresponding to the radial borehole azimuths of 15° , 30° and 45° are respectively 0.014, 0.026, 0.037, which shows that under the conditions of horizontal in-situ stress differences of 5 MPa, well length of 20 m and borehole diameter of 0.05 m, the radial boreholes with azimuths between 15° and 45° can create a guiding effect. Moreover, the guidance strength of the radial borehole decreases as the azimuth of the radial borehole increases. When the azimuth of a radial borehole increases by 30° , the guidance factor increases 2.6 times. When the azimuth of a radial borehole is 45° , the hydraulic fracture deflects and propagates along the maximum principle stress line after extending for 6.02 m. Thus, a single radial borehole with an azimuth of 45° does not significantly guide a hydraulic fracture to propagate along itself. Therefore, in order to make the research more practical, the follow-up studies take an azimuth angle of 30° as a basic condition.

4.2. Horizontal In-Situ Stress Differences

The main factor influencing propagation of fractures guided by radial boreholes is the horizontal in-situ stress difference, and radial boreholes could create enough guidance force to successfully guide a fracture only when the horizontal in-situ stress difference is within a certain range. In order to guarantee the validity of single factors, the influences of variable horizontal in-situ stress differences on fracture shape are analyzed, with a well length of 20 m, borehole diameter of 0.05 m, azimuth of 30° , maximum horizontal main stress $\sigma_H = 41$ MPa, and the same other parameters. The minimum horizontal main stresses are respectively 39, 36 and 33 MPa, and the simulation results are shown in Figure 7. The guidance factors corresponding to horizontal in-situ stress differences of 2, 5 and 8 MPa are respectively 0.010, 0.026, and 0.036, which shows that larger horizontal in-situ stress difference creates worse guidance strength of the radial borehole on the hydraulic fracture. Under the given parameters, when the horizontal in-situ stress difference is 8 MPa, the hydraulic fracture deflects and propagates along the maximum principle stress after extending for 7.53 m, with the smallest diversion radius and the largest deflection angle of fracture, and the weakest radial borehole guidance. When the horizontal in-situ stress difference is 5 MPa, the hydraulic fracture deflects and propagates along the maximum principle stress after extending for 10.12 m. Moreover, when the horizontal in-situ stress difference is 2 MPa, the hydraulic fracture diverts after extending for 18.50 m and propagates along the maximum main stress direction. The hydraulic fracture presents the largest diversion radius because it is affected by the radial borehole stress, and the deflection angle of the fracture is small and the guidance is obvious. When the horizontal in-situ stress difference increases by 6 MPa, the guidance factor increases 3.6 times. Therefore, in order to make the research more practical, the follow-up studies take the horizontal in-situ stress differences of 3 MPa as a basic condition to ensure an effective radial borehole guidance.

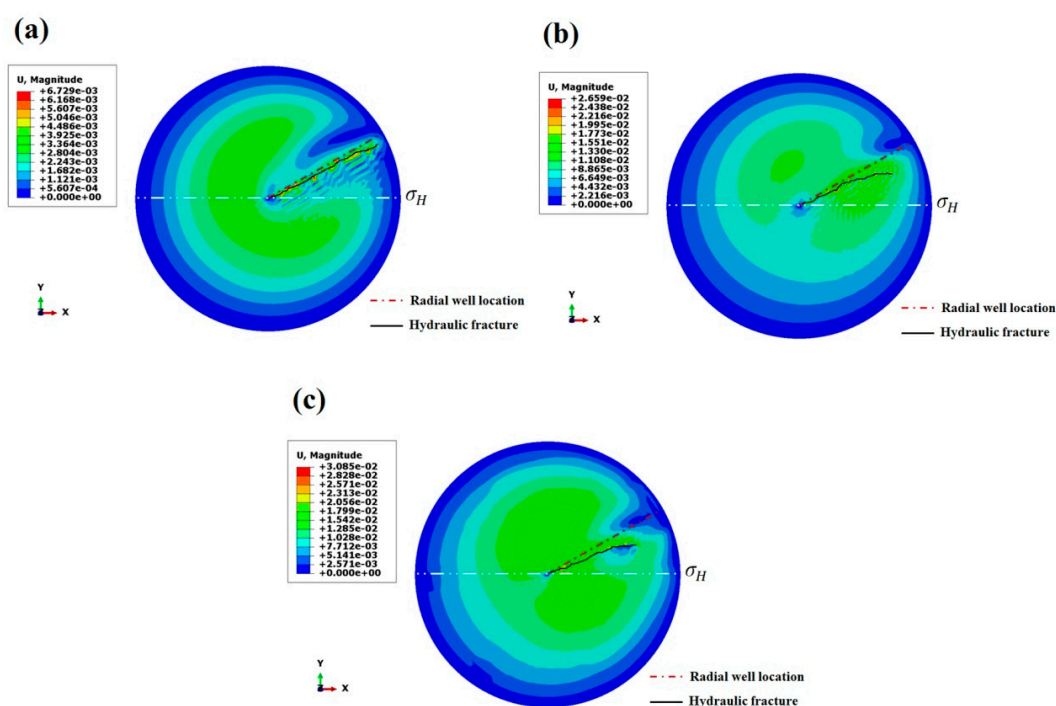


Figure 7. Simulation results of hydraulic fracture propagation guided by the single radial well under the different horizontal principal stress differences: (a) $\sigma_H = 39$ MPa; (b) $\sigma_H = 36$ MPa; and (c) $\sigma_H = 33$ MPa.

4.3. Radial Borehole Diameter

Models with radial borehole diameters (Φ) of 0.03, 0.05 and 0.07 m, horizontal principle stress difference of 3 MPa, and the same other parameters are established, and the computation results are shown in Figure 8. When the borehole diameter is 0.03 m, the hydraulic fracture deflects obviously

after extending for 8.13 m, with the smallest diversion radius and the largest fracture deflection angle. The guidance factor of a radial borehole with 0.03 m diameter is 0.036, which is a maximum and has the weakest guidance force among the three well radii. When the borehole diameter is 0.05 m, the hydraulic fracture deflects obviously after extending for 16.91 m. Its guidance factor is 0.015, and its guidance strength is larger than that of a 0.03 m radial borehole. The guidance factor of a 0.07 m radial borehole is 0.009, and the hydraulic fracture deflects obviously after extending for 18.03 m, which indicates the maximum guidance strength and the best guidance. Therefore, a larger radial borehole creates better fracture guidance. For this model, when the radial borehole diameter increases by 4 cm, the guidance factor decreases by 75%.

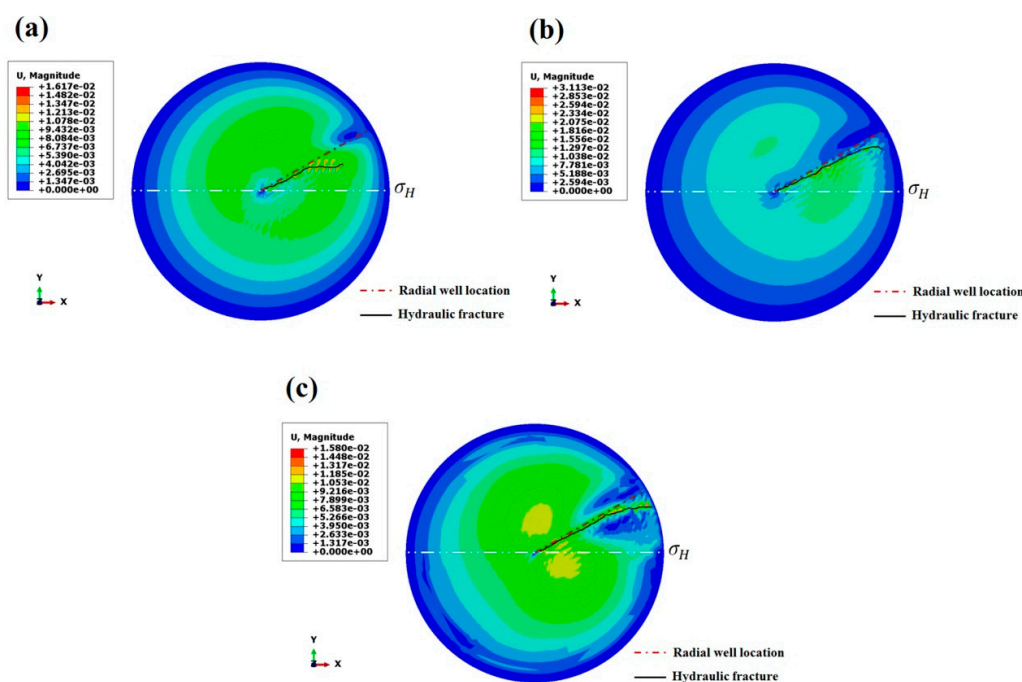


Figure 8. Simulation results of hydraulic fracture propagation guided by a single radial well under radial well different diameters: (a) $\Phi = 0.03$ m; (b) $\Phi = 0.05$ m; and (c) $\Phi = 0.07$ m.

4.4. Length of Radial Borehole

The simulation results with radial borehole lengths of 10, 15 and 20 m are shown in Figure 9. The hydraulic fracture guided by a radial borehole with a length of 10 m deflects after extending for 6.22 m, and its guidance factor is 0.048. Moreover, the deflection distances for radial boreholes with lengths of 15 m and 20 m correspond to 12.81 m and 17.53 m, and their guidance factors are respectively 0.024 and 0.015. Thus, a longer radial borehole creates a longer hydraulic fracture propagation distance along the orientation of the radial borehole, which could prevent early deflection of fractures towards the maximum principle stress and cause better guidance. The guidance factor decreases by about 69% for every increase of the radial borehole length by 10 m.

4.5. Young's Modulus of Reservoir Rock

The models with Young's modulus of 13, 23 and 33 GPa are established to analyze the influence of Young's modulus on the propagation of hydraulic fractures, and the simulation results are shown in Figure 10. When the Young's modulus is 13 GPa, the hydraulic fracture deflects after extending for 17.50 m along the radial borehole orientation, and its guidance factor is 0.015, which has the strongest guidance strength among three Young's modulus.

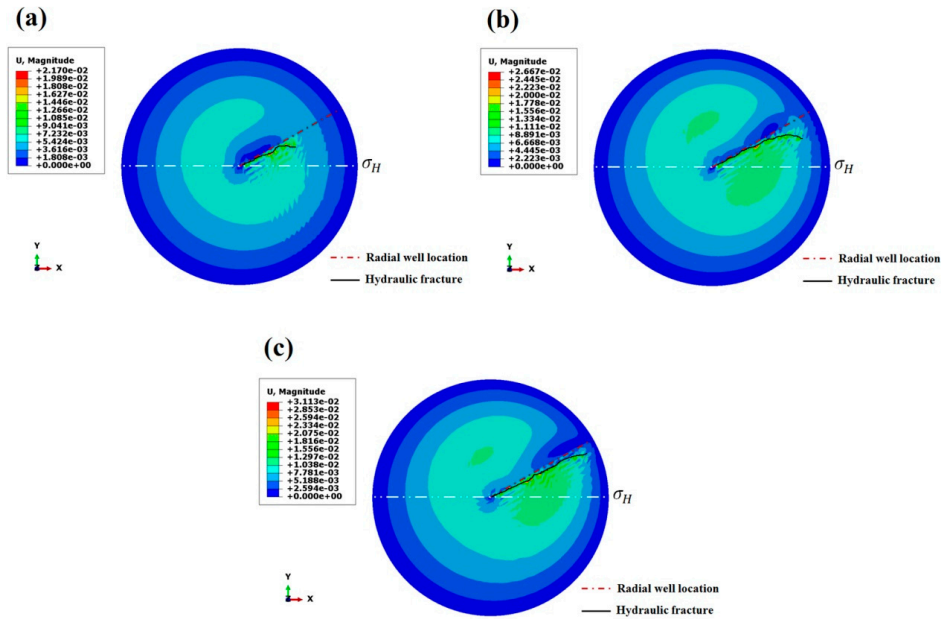


Figure 9. Simulation results of hydraulic fracture propagation guided by the single radial well under the different radial well lengths: (a) 10 m; (b) 15 m; and (c) 20 m.

When the Young’s modulus is 23 GPa, the hydraulic fracture deflects after extending for 16.94 m along the orientation of the radial borehole, and its guidance factor is 0.017. When the Young’s modulus is 33 GPa, the hydraulic fracture diverts after extending for 16.81 m along the radial borehole orientation, and its guidance factor is 0.018, which is the weakest guidance strength. When the Young’s modulus of reservoir rock increases by 20 GPa, the guidance factor increases by 20%. Thus, an increased Young’s modulus of the reservoir weakens the guidance of a radial borehole, but this weakening degree is really small.

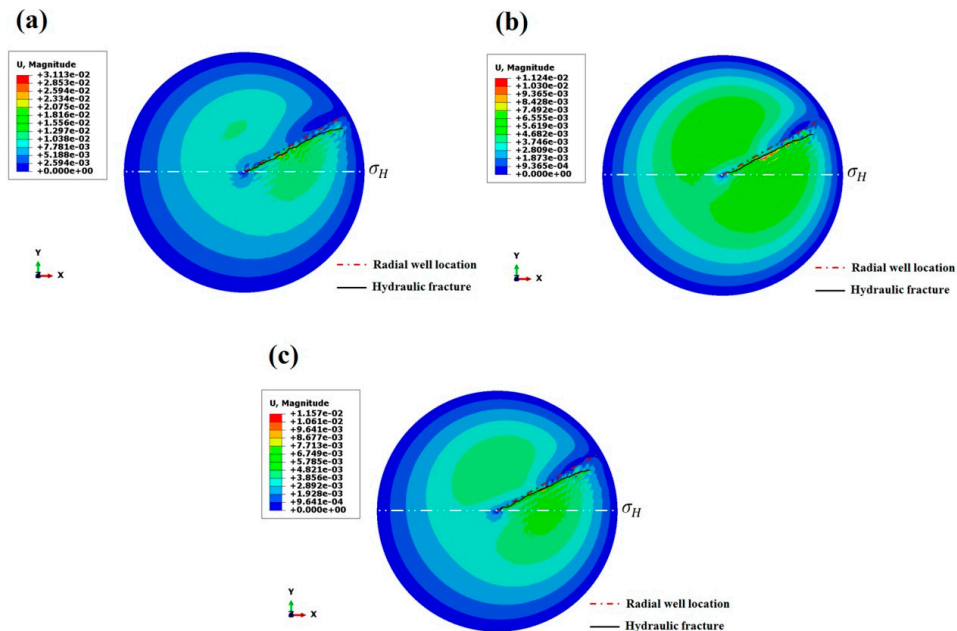


Figure 10. Simulation results of hydraulic fracture propagation guided by a single radial well under different Young’s modulus of reservoir rock: (a) 13 GPa; (b) 23 GPa; and (c) 33 GPa.

4.6. Poisson's Ratio of Reservoir Rock

Models with Poisson's ratios of 0.15, 0.20 and 0.25, and the same other parameters are established, and the simulation results are shown in Figure 11. When Poisson's ratio is 0.15, the hydraulic fracture deflects after extending for 14.53 m along the radial borehole orientation, and its guidance factor is 0.020, which has the weakest guidance strength. When Poisson's ratio is 0.20, the hydraulic fracture deflects after extending for 16.32 m along the radial borehole orientation, and its guidance factor is 0.016. When Poisson's ratio is 0.25, the hydraulic fracture deflects after extending for 17.54 m along the radial borehole orientation of, and its guidance factor is 0.015, which is the strongest guidance strength. When the Poisson's ratio of reservoir rock increases by 0.1, the guidance factor decreases by 25%. Thus, the increased Poisson's modulus of reservoir strengthens the guidance of a radial borehole and creates better guidance for hydraulic fracture propagation, but this impact is very weak.

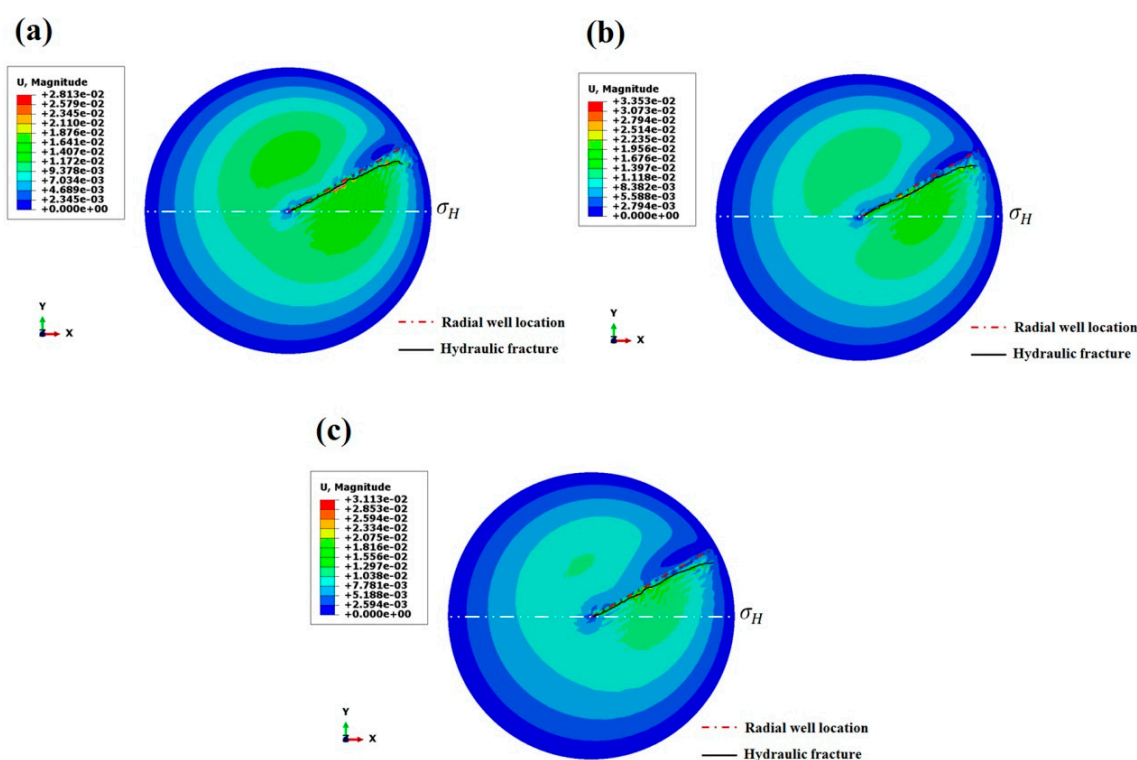


Figure 11. Simulation results of hydraulic fracture propagation guided by a single radial well under different Poisson ratios of reservoir rock: (a) 0.15; (b) 0.2; and (c) 0.25.

4.7. Reservoir Permeability

Models with reservoir permeability of $1 \times 10^{-3} \mu\text{m}^2$, $10 \times 10^{-3} \mu\text{m}^2$ and $100 \times 10^{-3} \mu\text{m}^2$, and the same other parameters were established, and the simulation results are shown in Figure 12. When the reservoir permeability is $1 \times 10^{-3} \mu\text{m}^2$, the hydraulic fracture basically propagates along the orientation of the radial borehole without deflection, and its guidance factor is 0.004, which is the strongest guidance strength. When the reservoir permeability is $10 \times 10^{-3} \mu\text{m}^2$, the hydraulic fracture also propagates along the radial borehole orientation without obvious deflection, and its guidance factor is 0.010, and its distance between hydraulic fracture and radial borehole is larger than that of the model with $1 \times 10^{-3} \mu\text{m}^2$ reservoir permeability. When the reservoir permeability is $100 \times 10^{-3} \mu\text{m}^2$, the hydraulic fracture deflects after extending for 16.72 m, and its guidance factor is 0.017, which represents the weakest guidance strength. When the reservoir permeability increases by 100 times, the guiding factor increases 4.3 times as much. Thus, the increased reservoir permeability weakens the radial borehole guidance. The smaller permeability tends to create a pressured area around the radial borehole and guide the propagation of a hydraulic fracture toward an ideal orientation.

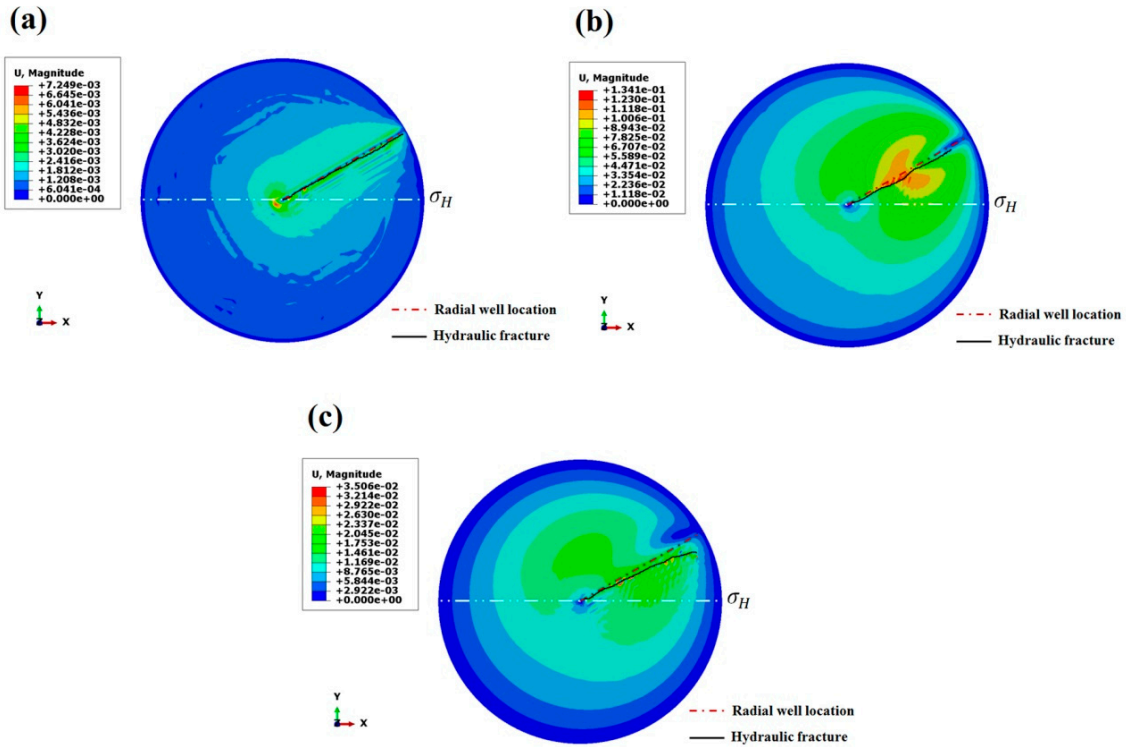


Figure 12. Simulation results of hydraulic fracture propagation guided by a single radial well under different reservoir permeabilities: (a) $1 \times 10^{-3} \mu\text{m}^2$; (b) $10 \times 10^{-3} \mu\text{m}^2$; and (c) $100 \times 10^{-3} \mu\text{m}^2$.

4.8. Fracturing Fluid Viscosity

Models with fracturing fluid viscosities of 1, 50, 100 and 150 mPa·s are established to analyze the influence of viscosity of fracturing fluid on propagation of hydraulic fracture, and the simulation results are shown in Figure 13.

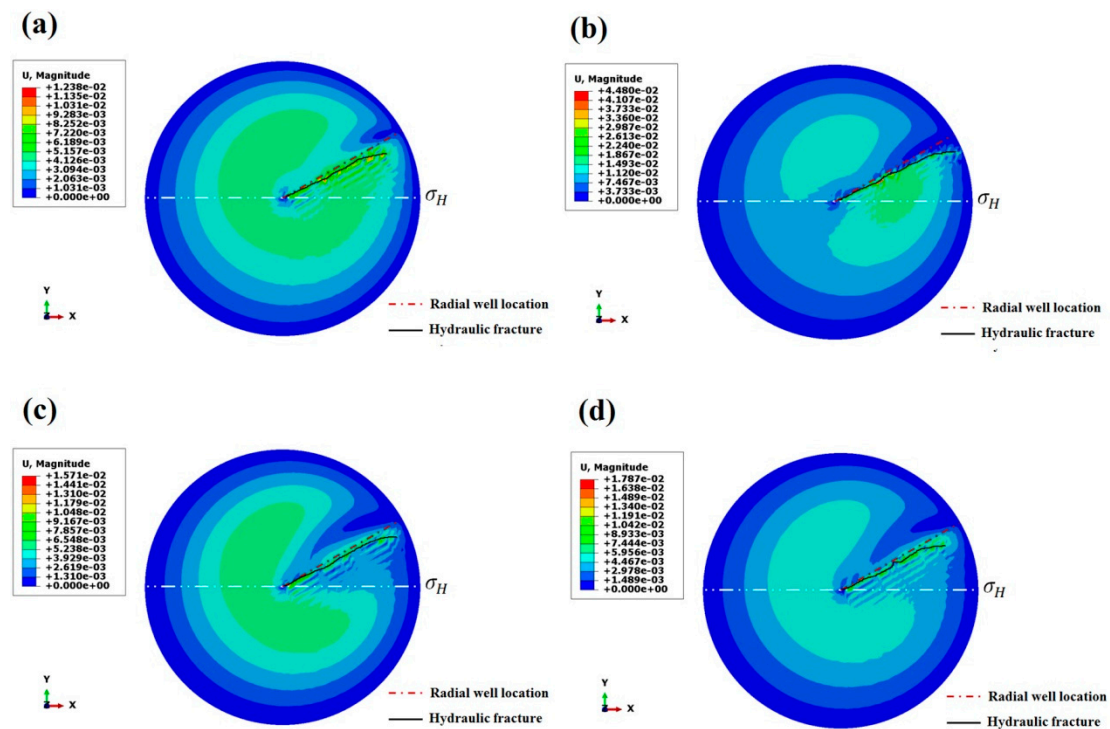


Figure 13. Simulation results of hydraulic fracture propagation guided by a single radial well under different fracturing fluid viscosities: (a) 1 mPa·s; (b) 50 mPa·s; (c) 100 mPa·s; and (d) 150 mPa·s.

When the viscosity of the fracturing fluid is 1 mPa·s, the hydraulic fracture deflects after extending 14.60 m along the radial borehole orientation, and its guidance factor is 0.021, which is the weakest guidance strength among the four viscosities. When the fracturing fluid viscosity is 50 mPa·s, the hydraulic fracture deflects after extending for 17.33 m, and its guidance factor is 0.008, which represents a very strong guidance strength. When the fracturing fluid viscosity is 100 mPa·s, the hydraulic fracture deflects after extending for 17.94 m, and its guidance factor is 0.007, which is the best guidance strength. When the fracturing fluid viscosity is 150 mPa·s, the radial borehole guidance continues to decrease and the hydraulic fracture deflects after extending for 15.31 m, and its guidance factor is 0.016. Thus, the fracturing fluid viscosity serves a dual function, both excessively high and low viscosity go against radial borehole guidance of a hydraulic fracture, and a fracturing fluid viscosity of 50–100 mPa·s creates the best guidance for hydraulic fracture propagation.

4.9. Fracturing Fluid Injection Rate

Models with fracturing fluid injection rates of 1, 3, 6 and 9 m³/min were established to analyze the influence of fracturing fluid injection rate on hydraulic fracture propagation, and the simulation results are shown in Figure 14. When the injection rate fracturing fluid is 1 m³/min, the hydraulic fracture deflects after extending 13.12 m along the radial borehole orientation, and its guidance factor is 0.023, which is the weakest guidance strength among the four injection rates. When the fracturing fluid injection rate is 3 m³/min, the hydraulic fracture deflects after extending 15.71 m, and its guidance factor is 0.018. When the fracturing fluid injection rate is 6 m³/min, the hydraulic fracture deflects after extending for 17.14 m, and its guidance factor is 0.011. When the fracturing fluid injection rate is 9 m³/min, the hydraulic fracture basically propagates along the radial borehole orientation without deflection, and its guidance factor is 0.002. When the fracturing fluid injection rate increases by 8 m³/min, the guiding factor decreases by about 91%. Thus, an increased fracturing fluid injection rate strengthens the radial borehole guidance and creates better guidance for hydraulic fracture propagation. This conclusion is a very important basis for guiding field fracturing.

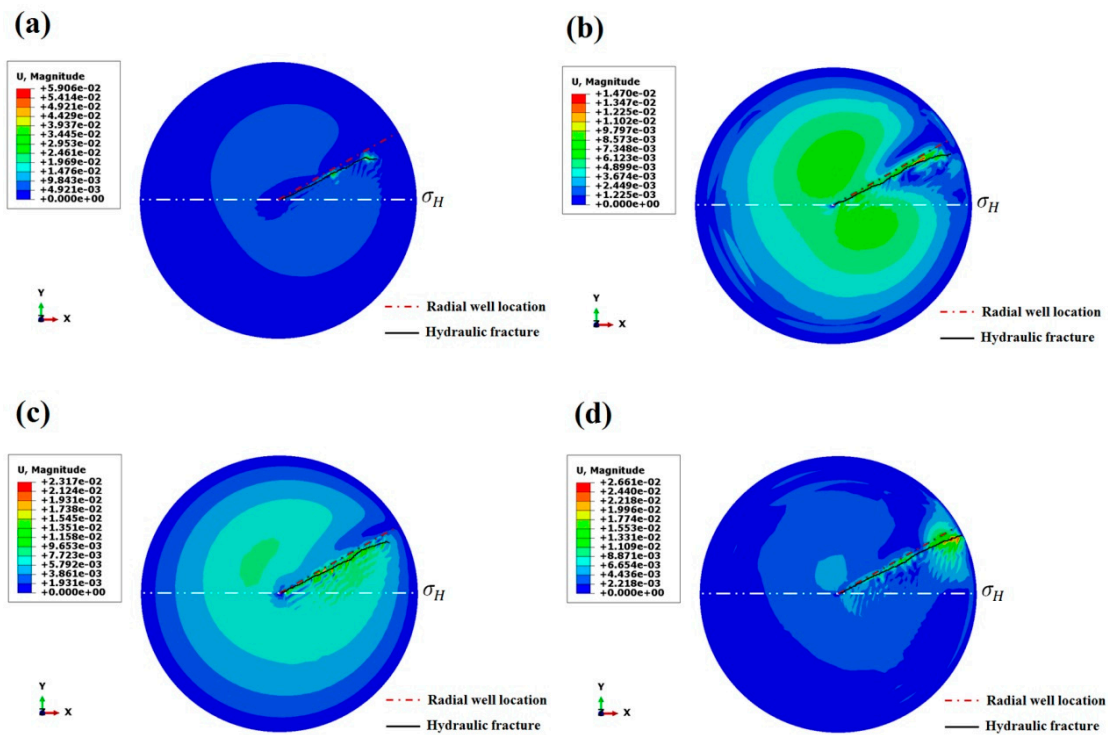


Figure 14. Simulation results of hydraulic fracture propagation guided by the single radial well under the different fracturing fluid injection rates: (a) 1 m³/min; (b) 3 m³/min; (c) 6 m³/min; and (d) 9 m³/min.

4.10. Gray Correlation Analysis of Guidance Factors

Gray correlation analysis [35] is a mathematical method that measures the interdependence of influence factors based on the similarity and diversity of variation trends of studied factors. The application of the gray correlation analysis method is described as follows: first, the various parameters need to be treated with dimensionless equalization according to Equation (8), and then the gray correlation coefficients are obtained according to Equation (9). Finally, the correlation degrees are calculated according to Equation (10):

$$X_i(k) = \frac{x_i(k)}{\bar{x}_i} \quad i = 1, 2, \dots, m; k = 1, 2, \dots, N \quad (17)$$

$$\xi_i(k) = \frac{\min_i \min_k |X_o(k) - X_i(k)| + \rho \max_i \max_k |X_o(k) - X_i(k)|}{|X_o(k) - X_i(k)| + \rho \max_i \max_k |X_o(k) - X_i(k)|} \quad (18)$$

$$\gamma_i = \frac{1}{N} \sum_{k=1}^N \xi_i(k) \quad (19)$$

where $X_i(k)$ is the dimensionless equalization value of the i -th parameter. i is the parameter number. k is the data number. $x_i(k)$ is the i -th parameter value. \bar{x}_i is the arithmetic mean of $x_i(1), x_i(2), \dots, x_i(N)$. m is the number of parameters. N is the number of data. $\xi_i(k)$ is the gray correlation coefficient. $X_o(k)$ and $X_i(k)$ are the dimensionless equalization values of reference sequence and comparative sequence, respectively. ρ is the distinguishing coefficient, its value is generally 0.5. γ_i is the correlation degree.

Nine factors influencing the guidance to hydraulic fracture are treated with dimensionless equalization by gray correlation analysis, and the correlation coefficients between these factors and the 'guidance factor' are calculated, and their influence is comprehensively analyzed. The evaluation results are shown in Table 2.

Table 2. Gray correlation coefficient corresponding to different parameters.

No.	Parameters	Correlation Coefficient
1	Radial well azimuth	0.7680
2	Radial well diameter	0.7537
3	Radial well length	0.7485
4	Horizontal principal stress difference	0.7921
5	Young's modulus of rock	0.7465
6	Poisson ratio of rock	0.5312
7	Reservoir permeability	0.7367
8	Fracturing fluid viscosity	0.7354
9	Injection rate of fracturing fluid	0.7476

The gray correlation analysis shows that the correlation between the horizontal in-situ stress difference and 'guidance factor' is primary, and the correlation factor is 0.7921, which shows that the guidance strength of radial borehole is most influenced by the change of horizontal in-situ stress difference. The correlation coefficient of radial borehole azimuth is 0.7680, which takes second place, and it shows that azimuth of radial borehole is also an important factor that influences guidance. The correlation coefficient of borehole diameter of radial borehole is 0.7537, which takes third place, and it is also an important factor influencing guidance. The correlation coefficient of Poisson's ratio is 0.5312, which is the weakest factor. It is shown that the guidance of radial boreholes on hydraulic

fractures is least influenced. The result of gray correlation analysis shows that the influences level (from strong to weak) of the above factors on guidance strength of a single radial borehole can be listed as follows: horizontal in-situ stress differences > azimuth of radial borehole > radial borehole diameter > length of radial borehole > fracturing fluid injection rate > Young modulus of rock > reservoir permeability > fracturing fluid viscosity > Poisson's ratio. A large amount of simulation shows that the parameters of radial borehole, physical property parameters of reservoir and fracturing operation parameters together influence the guidance of a single radial borehole.

5. Experimental Verification

In order to verify the feasibility of directional propagation of hydraulic fracturing guided by the single radial borehole, two sets of true triaxial hydraulic fracturing simulation experiments were carried out for large-size artificial cores (300 mm³) [36]. The rock mechanics test results of the artificial cores show an average Young modulus of 14 GPa, average Poisson's ratio of 0.22, and average tensile strength of 2.7 MPa. The vertical borehole is modeled with a steel tube, which has an OD of 28 mm, ID of 23 mm, and length of 270 mm. In order to model an open radial borehole resulting from a radial hydraulic jet, and guarantee unlikely deformation of pre-set radial boreholes while pouring cement mortar, a polytetrafluoroethylene (PTFE) tube is chosen to model the radial borehole after several trials, and a combination of drilling holes and cutting sieves in PTFE tube is adopted to obtain properties close to those of actual radial boreholes, which not only ensures enough strength to prevent deformation and stop cement mortar flowing into the PTFE tube when casting specimens, but also guarantees enough flowing channel. The PTFE tube has a length of 130 mm, and a diameter of 10 mm, is preset in the modeling wellbore.

Hydraulic fracturing experiments by the single radial borehole are modeled for 1# and 2# cores with radial borehole azimuth of 15° and horizontal in-situ stress differences of 3 and 6 MPa respectively, and the modeling results are shown in Figures 15 and 16. For the 1# core, the hydraulic fracture initiates in the heel of the radial borehole, with a fracture height and fracture length propagated along the radial borehole, forming a fracture with a relatively flat plane (Figure 15a). At the side of the non-radial borehole, the hydraulic fracture propagates along the maximum horizontal geostress (Figure 15b). The results show that with a smaller radial borehole azimuth (15°) and smaller horizontal in-situ stress difference (3 MPa), the single radial borehole has a significant influence on the propagation of fractures, and creates strong guidance for the directional propagation of hydraulic fractures. For the 2# core with a horizontal in-situ stress difference of 6 MPa, the surface of the fractured core shows complicated fractures (Figure 16a), which initiate in the heel of radial borehole (Figure 16b). However, due to the larger horizontal in-situ stress difference, the fracture propagates along the radial borehole firstly in the direction of the fracture length and deflects at the position of 6 cm, and basically propagates along the horizontal maximum geostress when approaching the core boundary. Controlled by a large horizontal in-situ stress difference, the fracture height cannot effectively propagate in the plane, but distorts from the radial borehole azimuth to the direction of horizontal maximum geostress, and it is nearly parallel to the maximum horizontal principal stress on the surface of the core, forming a wedge-shape fracture. In addition, affected by the mutual interference from radial boreholes and horizontal geostress, multi-branch fractures occur in the core under the modeling conditions, forming complicated fractures, as shown in Figures 16(c–e).

Comparison of the fractures in the 1# and 2# cores show that the guidance of a single radial borehole on hydraulic fracture propagation is limited by the radial borehole azimuth and horizontal geostress difference. A single radial borehole with larger azimuth and larger horizontal in-situ stress difference has poor guidance of the directional propagation of hydraulic fractures. Due to the complex operation, heavy workload, and long experimental period in large size physical modeling of true tri-axial hydraulic fracturing, only two groups of experiments were carried out, but the experimental results are consistent with the numerical simulation results, which shows that the numerical simulation results are reliable to some extent.

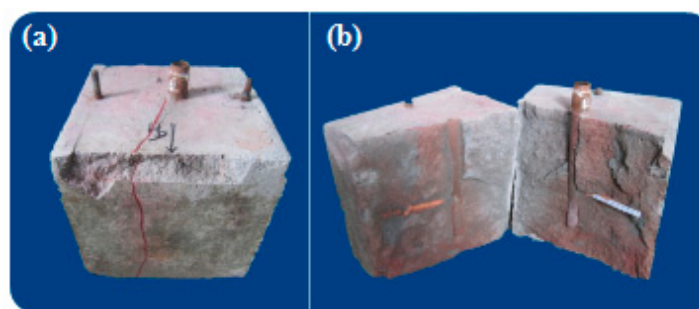


Figure 15. Fracture morphology after hydraulic fracturing of sample 1#: (a) the overall picture before opening; (b) the inner picture after opening.

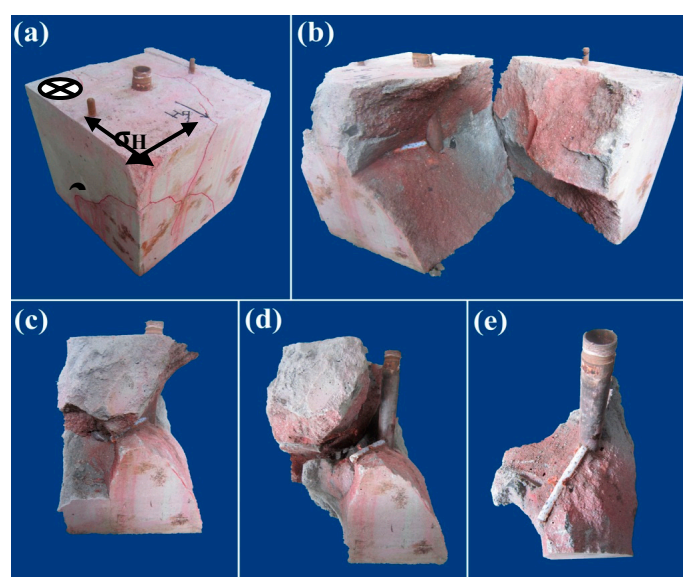


Figure 16. Fracture morphology after hydraulic fracturing of sample 2#: (a) the overall picture before opening; (b) the fracture initiates in the heel of radial borehole; (c–e) the multi-branch fractures occur in the core.

6. Conclusions and Suggestions for Future Work

The paper aimed to provide theoretical support for the artificial control technology of directional propagation of hydraulic fracture guided by a single radial borehole. A 3D extended finite-element numerical model of hydraulic fracturing guided by a single radial borehole is established by using the Abaqus Software. The numerical simulation results were as follows:

- (1) The influence of in-situ stress could be overcome by scientifically arranging the single radial borehole under certain reservoir conditions, which realizes directional propagation towards target area. Thus, the problem that the hydraulic fracture only propagates along the direction parallel to horizontal maximum in-situ stress, and the available wellbores fail to develop the remaining oil and trap reservoir, and complex multi-fractures tend to generate in the immediate vicinity of wellbore, which makes it hard to realize the deep penetration of fractures, are solved to improve the effectiveness of fracturing operations and recovery efficiency in oil fields.
- (2) The concept of ‘guidance factor’ is introduced for the first time to quantify the guidance of a radial borehole on hydraulic fractures. A large amount of simulation shows that the ‘guidance factor’ reflects the guidance of a radial borehole on hydraulic fractures, and larger guidance factor reflects weaker guidance strength.
- (3) A smaller radial borehole azimuth, horizontal in-situ stress difference and larger radial borehole diameter and length create stronger guidance strength, and vice versa. When the azimuth of the radial borehole increases from 15° to 45°, the guidance factor increases 2.6 times as much; when

the horizontal in-situ stress difference increases from 2 MPa to 8 MPa, the guidance factor increases 3.6 times; when the wellbore diameter increases from 3 cm to 7 cm, the guidance factor decreases 75%; when the well length increases from 10 m to 20 m, the guidance factor decreases 69%.

- (4) Both reservoir physical properties and fracturing operation parameters influence the guidance of radial boreholes on hydraulic fractures. The increased Poisson's ratio and injection rate strengthen the radial borehole guidance, and the increased Young modulus and permeability weaken the radial borehole guidance, both excessive high and low viscosity go against radial borehole guidance of hydraulic fractures, and a fracturing fluid viscosity between 50–100 mPa·s creates the best guidance on propagation of hydraulic fractures.
- (5) The gray correlation analysis results show that the influence level (from strong to weak) of the above factors on radial borehole guidance may be listed as follows: horizontal in-situ stress differences > azimuth > borehole diameter > length > fracturing fluid injection rate > Young modulus of rock > reservoir permeability > fracturing fluid viscosity > Poisson's ratio. The parameters of the radial borehole, physical property parameters of the reservoir and fracturing operation parameters together influence the guidance strength of a radial borehole on hydraulic fractures.
- (6) The numerical model is based on real rock parameters from a practical field. It is recommended that the numerical model of different fields and areas should be established based on their rock physical mechanical parameters, and the influence of different factors on guidance be analyzed to obtain radial borehole parameters and fracturing operation parameters applicable to their conditions, which is beneficial to improving the fracturing success rate.
- (7) The experimental results show that the guidance of a single radial borehole on hydraulic fracture propagation is limited by the radial borehole azimuth and horizontal in-situ stress difference. A single radial borehole with larger azimuth and larger horizontal in-situ stress difference has poor guidance of the directional propagation of hydraulic fractures. The experimental results are consistent with the numerical simulation results, which shows that the numerical simulation results are reliable to some extent.

Acknowledgments: The authors would like to acknowledge the financial support of the National Natural Science Foundation of China (Grant No. 51404288), the Fundamental Research Funds for the Central Universities (Grant No. 17CX02077) and the Applied Basic Research Project for Qingdao (Grant No. 17-1-1-20-jch).

Author Contributions: Tiankui Guo and Zhanqing Qu established the numerical model and designed the research; Facheng Gong and Xiaozhi Wang performed the research and analyzed simulation results.

Conflicts of Interest: The authors declare that they have no competing interests.

References

1. Dickinson, W.; Dykstra, H.; Nees, J.M.; Dickinson, E. The ultra-short radius radial system applied to thermal recovery of heavy oil. In Proceedings of the SPE Western Regional Meeting, Bakersfield, CA, USA, 30 March–1 April 1992.
2. Li, Y.H.; Wang, C.J.; Shi, L.H.; Guo, W.Y. Application and development of drilling and completion of the ultra short-radius radial well by high pressure jet flow techniques. In Proceedings of the International Oil and Gas Conference and Exhibition, Beijing, China, 7–10 November 2000.
3. Gong, D.G.; Qu, Z.Q.; Guo, T.K.; Tian, Y.; Tian, K.H. Variation rules of fracture initiation pressure and fracture starting point of hydraulic fracture in radial well. *J. Pet. Sci. Eng.* **2016**, *140*, 41–56.
4. Ursegov, S.; Bazylev, A.; Taraskin, E. First results of cyclic stimulations of vertical wells with radial horizontal bores in heavy oil carbonates (Russian). In Proceedings of the SPE Russian Oil and Gas Technical Conference and Exhibition, Moscow, Russia, 28–30 October 2008.
5. Megorden, M.P.; Jiang, H.; Bentley, P.J.D. Improving hydraulic fracture geometry by directional drilling in a coal seam gas formation. In Proceedings of the SPE Unconventional Resources Conference and Exhibition-Asia Pacific, Brisbane, Australia, 11–13 November 2013.
6. Guo, T.K.; Li, Y.C.; Ding, Y.; Qu, Z.Q.; Gai, N.C.; Rui, Z.H. Evaluation of acid fracturing treatments in shale formation. *Energy Fuels* **2017**, *31*, 10479–10489.

7. Zhang, X.; Jeffrey, R.G.; Bungler, A.P.; Thiercelin, M. Initiation and growth of a hydraulic fracture from a circular wellbore. *Int. J. Rock Mech. Min. Sci.* **2012**, *48*, 984–995.
8. Cherny, S.G.; Lapin, V.N.; Chirkov, D.V.; Alekseenko, O.; Medvedev, O.O. 2D modeling of hydraulic fracture initiating at a wellbore with or without microannulus. In Proceedings of the SPE Hydraulic Fracturing Technology Conference, The Woodlands, TX, USA, 19–21 January 2009.
9. Yuan, Y.; Abousleiman, Y.; Weng, X. Three-dimensional elastic analysis on fracture initiation from a perforated borehole. In Proceedings of the Low Permeability Reservoirs Symposium, Denver, CO, USA, 19–22 March 1995.
10. Alekseenko, O.P.; Potapenko, D.I.; Cherny, S.G.; Esipov, D.; Kuranakov, D.; Lapin, V. 3-D modeling of fracture initiation from perforated non-cemented wellbore. In Proceedings of the SPE Hydraulic Fracturing Technology Conference, The Woodlands, TX, USA, 6–8 February 2012.
11. Zhu, H.; Deng, J.; Jin, X.; Hu, L.B.; Luo, B. Hydraulic fracture initiation and propagation from wellbore with oriented perforation. *Rock Mech. Rock Eng.* **2015**, *48*, 585–601.
12. Lei, X.; Zhang, S.C.; Xu, G.Q.; Zou, Y.S. Impact of perforation on hydraulic fracture initiation and extension in tight natural gas reservoirs. *Energy Technol.* **2015**, *3*, 618–624.
13. Fallahzadeh, S.H.; Rasouli, V.; Sarmadivaleh, M. An investigation of hydraulic fracturing initiation and near-wellbore propagation from perforated boreholes in tight formations. *Rock Mech. Rock Eng.* **2015**, *48*, 573–584.
14. Chen, M.; Jiang, H.; Zhang, G.Q.; Jin, Y. The experimental investigation of fracture propagation behavior and fracture geometry in hydraulic fracturing through oriented perforations. *Pet. Sci. Technol.* **2010**, *28*, 1297–1306.
15. Hong, J.M.; Shin, S.R.; Lim, J.S.; Jeong, W.K.; Jang, W.Y. A study on the model for effective hydraulic fracturing by using guide Hole. *Tunn. Undergr. Space* **2014**, *24*, 440–448.
16. Gunde, A.C.; Bera, B.; Mitra, S.K. Investigation of water and CO₂ (carbon dioxide) flooding using micro-CT (micro-computed tomography) images of Berea sandstone core using finite element simulations. *Energy* **2010**, *35*, 5209–5216.
17. Fries, T.P.; Belytschko, T. The extended/generalized finite element method: An overview of the method and its applications. *Int. J. Numer. Methods Eng.* **2010**, *84*, 253–304.
18. Dong, Y.W.; Ren, Q.W. An extended finite element method for modeling hydraulic fracturing in gravity dam. *J. Hydraul. Eng.* **2011**, *42*, 1361–1367.
19. Gordeliy, E.; Peirce, A. Coupling schemes for modeling hydraulic fracture propagation using the XFEM. *Comput. Methods Appl. Mech. Eng.* **2012**, *253*, 305–322.
20. Wang, T.; Gao, Y.; Liu, Z.L.; Wang, Y.H.; Yang, L.F.; Zhuang, Z. Numerical simulations of hydraulic fracturing in large objects using an extended finite element method. *J. Tsinghua Univ. (Sci. Technol.)* **2014**, *54*, 1304–1309.
21. He, J.M.; Zhang, Z.B.; Li, X. Numerical analysis on the formation of fracture network during the hydraulic fracturing of shale with pre-existing fractures. *Energies* **2017**, *10*, 736.
22. Moës, N.; Belytschko, T. Extended finite element method for cohesive crack growth. *Eng. Fract. Mech.* **2002**, *69*, 813–833.
23. Rui, Z.; Lu, J.; Zhang, Z.; Guo, R.; Ling, K.; Zhang, R.; Patil, S. A quantitative oil and gas reservoir evaluation system for development. *J. Nat. Gas Sci. Eng.* **2017**, *42*, 31–39.
24. Meixner, J.; Schill, E.; Grimmer, J.C.; Gaucher, E.; Kohl, T.; Klingler, P. Structural control of geothermal reservoirs in extensional tectonic settings: An example from the Upper Rhine Graben. *J. Struct. Geol.* **2016**, *82*, 1–15.
25. Zhang, Y.J.; Li, Z.W.; Guo, L.L.; Gao, P.; Jin, X.P. Electricity generation from enhanced geothermal systems by oilfield produced water circulating through reservoir stimulated by staged fracturing technology for horizontal wells: A case study in Xujiaweizi area in Daqing Oilfield, China. *Energy* **2014**, *78*, 788–805.
26. Tang, C.A.; Tham, L.G.; Lee, P.K.K.; Yang, T.H.; Li, L.C. Coupled analysis of flow, stress and damage (FSD) in rock failure. *Int. J. Rock Mech. Min. Sci.* **2002**, *39*, 477–489.
27. Chen, W.Z.; Wu, G.J.; Jia, S.P. *The Application of Abaqus in Tunnels and Underground Engineering*, 1st ed.; China Water & Power Press: Beijing, China, 2009; pp. 228–235, ISBN 978-7-5084-6995-9.
28. Guo, L.L.; Chen, Z.F.; Luo, J.R.; Chen, G. A review of the extended finite element method and its applications. *Chin. Q. Mech.* **2011**, *2*, 612–625.

29. Yue, Q.X.; Li, J. A research on saturated soil dynamic response with ABAQUS. *Earthq. Eng. Eng. Vib.* **2006**, *26*, 238–241.
30. Sepehri, J.; Soliman, M.Y.; Morse, S.M. Application of extended finite element method (XFEM) to simulate hydraulic fracture propagation from oriented perforations. In Proceedings of the SPE Hydraulic Fracturing Technology Conference, The Woodlands, TX, USA, 3–5 February 2015.
31. Kachanov, L.M. Time of the rupture process under creep conditions. *Izv. Akad. Nauk. SSR* **1958**, *8*, 26–31.
32. Haddad, M.; Sepehrnoori, K. XFEM-based CZM for the simulation of 3D multiple-stage hydraulic fracturing in quasi-brittle shale formations. In Proceedings of the 49th US Rock Mechanics/Geomechanics Symposium, San Francisco, CA, USA, 28 June–1 July 2015.
33. Remmers, J.J.C.; Borst, R.D.; Needleman, A. The simulation of dynamic crack propagation using the cohesive segments method. *J. Mech. Phys. Solids* **2008**, *56*, 70–92.
34. Zhang, G.Q.; Chen, M.; Zhao, Y.B. Study on initiation and propagation mechanism of fractures in oriented perforation of new wells. *Acta Pet. Sin.* **2008**, *29*, 116–119.
35. Kadier, A.; Abdeshahian, P.; Simayi, Y.; Ismail, M.; Hamid, A.A.; Kalil, M.S. Gray relational analysis for comparative assessment of different cathode materials in microbial electrolysis cells. *Energy* **2015**, *90*, 1556–1562.
36. Fallahzadeh, S.H.; Hossain, M.M.; Cornwell, A.J.; Rasouli, V. Near wellbore hydraulic fracture propagation from perforations in tight rocks: The roles of fracturing fluid viscosity and injection rate. *Energies* **2017**, *10*, 359.



© 2017 by the authors. Licensee MDPI, Basel, Switzerland. This article is an open access article distributed under the terms and conditions of the Creative Commons Attribution (CC BY) license (<http://creativecommons.org/licenses/by/4.0/>).